

Quantum squeezing and sensing with pseudo anti-parity-time symmetry

Xi-Wang Luo,¹ Chuanwei Zhang,^{1,*} and Shengwang Du^{1,†}

¹*Department of Physics, The University of Texas at Dallas, Richardson, Texas 75080-3021, USA*

The emergence of parity-time (\mathcal{PT}) symmetry has greatly enriched our study of symmetry-enabled non-Hermitian physics, but the realization of quantum \mathcal{PT} -symmetry faces an intrinsic issue of unavoidable symmetry-breaking Langevin noises. Here we construct a quantum pseudo-anti- \mathcal{PT} (pseudo- \mathcal{APT}) symmetry in a two-mode bosonic system without involving Langevin noises. We show that the spontaneous pseudo- \mathcal{APT} symmetry breaking leads to an exceptional point, across which there is a transition between different types of quantum squeezing dynamics, *i.e.*, the squeezing factor increases exponentially (oscillates periodically) with time in the pseudo- \mathcal{APT} symmetric (broken) region. Such dramatic changes of squeezing factors and quantum dynamics near the exceptional point are utilized for ultra-precision quantum sensing. These exotic quantum phenomena and sensing applications can be experimentally observed in two physical systems: spontaneous wave mixing nonlinear optics and atomic Bose-Einstein condensates. Our work offers a physical platform for investigating exciting \mathcal{APT} symmetry physics in the quantum realm, paving the way for exploring fundamental quantum non-Hermitian effects and their quantum technological applications.

Introduction.—Hermiticity and real eigenvalues of a Hamiltonian are key postulates of quantum mechanics. While non-Hermitian Hamiltonians emerged from the interaction with external environments generally possess complex eigenspectra, they can exhibit entirely real eigenvalues in the presence of parity-time (\mathcal{PT}) symmetry [1–7]. When the non-Hermiticity parameter exceeds a critical value, known as exceptional point (EP), the \mathcal{PT} -symmetry can be spontaneously broken for the eigenstates, leading to a phase transition from the \mathcal{PT} -symmetric phase with purely real eigenvalues to the \mathcal{PT} -broken phase with complex conjugate eigenvalue pairs. In the past decade, significant experimental and theoretical progress [8–20] has been made for exploring \mathcal{PT} -symmetry physics in various physical systems (e.g., photonics, acoustics, ultracold atoms, etc.), which generally utilize the control of linear gain/loss in classical wave systems. However, an intrinsic issue for studying \mathcal{PT} -symmetry physics in the quantum realm [21–27] is that a \mathcal{PT} -symmetric Hamiltonian involving linear gain/loss does not preserve the commutation relations of quantum field operators, therefore Langevin noises, which break \mathcal{PT} symmetry, must be included in quantum systems [28]. Two experimental approaches to circumvent this issue for quantum \mathcal{PT} -symmetry include discarding quantum noise through post-selection measurement [25] and Hamiltonian dilation by embedding a non-Hermitian Hamiltonian into a larger Hermitian system [26].

Anti- \mathcal{PT} (\mathcal{APT}) represents another non-Hermitian symmetry with the Hamiltonian *anticommuting* with \mathcal{PT} operator (*i.e.*, $\{H_{\mathcal{APT}}, \mathcal{PT}\} = 0$ instead of commutation $[H_{\mathcal{PT}}, \mathcal{PT}] = 0$ for \mathcal{PT} -symmetry) and has recently attracted great interests [29–38]. Similar as \mathcal{PT} symmetry, the spontaneous breaking of \mathcal{APT} symmetry also leads to the emergence of EPs. Recent studies showed that an \mathcal{APT} -symmetric system does not have to involve linear gain/loss of classical fields, making it possible to realize a quantum \mathcal{APT} -symmetry without Langevin noises

[36–38]. In this Letter, we construct a quantum \mathcal{APT} -symmetry in a two-mode bosonic system, where the dynamical Hamiltonian matrix is non-Hermitian and preserves the \mathcal{APT} -symmetry, while the second-quantized Hamiltonian is Hermitian. In this sense, we name it a pseudo- \mathcal{APT} symmetry. Our main results are:

i) The quantum pseudo- \mathcal{APT} -symmetry builds on coupling Bose creation operator of one field with the annihilation operator of the other field, yielding the Hermiticity of the second-quantized Hamiltonian that does not involve Langevin noises. The spontaneous \mathcal{APT} symmetry breaking across the EP for the dynamical Hamiltonian matrix yields a transition from purely imaginary (\mathcal{APT} -symmetric) to purely real (\mathcal{APT} -broken) eigenvalues, which is opposite to typical real to imaginary transition for the \mathcal{PT} -symmetry.

ii) Across the EP, the pseudo- \mathcal{APT} symmetry and quantized Hamiltonian yield a transition between different types of quantum squeezing dynamics. Specifically, the two-mode squeezing factor oscillates periodically with time in the pseudo- \mathcal{APT} -broken region, increases linearly at EP, and grows exponentially in the pseudo- \mathcal{APT} -symmetric region. Optical field squeezed states have been widely studied because of their fundamental interest (e.g., the implementation of EPR paradox) as well as broad applications in quantum information processing (e.g., continuous-variable quantum teleportation) and quantum metrology (e.g., gravitational wave detection) [39, 40]. Here the connection between pseudo- \mathcal{APT} -symmetry transition and different quantum squeezing dynamics is established.

iii) The dramatic changes of quantum squeezing factors and dynamics close to the EP make them ultra-sensitive to some parameters, thus can be utilized to achieve ultra-precision quantum sensing. In contrast to quantum sensing based on large squeezing factor [41, 42], here we focus on the \mathcal{APT} -broken region with weak squeezing that is usually undesirable in previous experi-

ments. We show that simple measurement schemes can reach the sensitivity close to the quantum Cramér-Rao bound given by the quantum Fisher information [41, 42], which exhibits divergent feature as the EP is approached. The squeezing factor is 1 at the working points, therefore the ultra-precision sensitivity originates from the pseudo- \mathcal{APT} symmetry rather than squeezing or entanglement.

iv) We propose that the connection between the quantum pseudo- \mathcal{APT} symmetry and the transition of squeezing dynamics as well as the ultra-precision quantum sensors can be realized experimentally in spontaneous wave mixing nonlinear optics and ultracold atomic Bose-Einstein condensates (BECs). In the BEC case, we establish the connection between the pseudo- \mathcal{APT} transition and the well-known transition to dynamical instability [43].

Pseudo- \mathcal{APT} -symmetry and quantum squeezing.— Consider a two-mode bosonic model described by the second-quantized Hermitian Hamiltonian

$$\mathcal{H} = \delta \left(\hat{a}_1^\dagger \hat{a}_1 + \hat{a}_2^\dagger \hat{a}_2 \right) + i\kappa \left(\hat{a}_1^\dagger \hat{a}_2^\dagger - \hat{a}_1 \hat{a}_2 \right), \quad (1)$$

where \hat{a}_j and \hat{a}_j^\dagger are the bosonic annihilation and creation operators, and the detuning δ and coupling coefficient κ are both real numbers. From Heisenberg equation, we obtain the dynamical equation (we set $\hbar = 1$) [44]

$$i\partial_t \left(\hat{a}_1, \hat{a}_2^\dagger \right)^T = H_{APT} \left(\hat{a}_1, \hat{a}_2^\dagger \right)^T, \quad (2)$$

with the non-Hermitian dynamical Hamiltonian matrix

$$H_{APT} = \delta\sigma_z + i\kappa\sigma_x = \begin{pmatrix} \delta & i\kappa \\ i\kappa & -\delta \end{pmatrix}. \quad (3)$$

H_{APT} satisfies $\{H_{APT}, \mathcal{PT}\} = 0$, with the parity operator $\mathcal{P} = \sigma_x$ and the time-reversal complex conjugate operator \mathcal{T} . In the pseudo- \mathcal{APT} -symmetric region (*i.e.*, the eigenstates of H_{APT} are \mathcal{PT} -symmetric) $|\delta| < |\kappa|$, H_{APT} has two imaginary eigenvalues $\lambda_\pm = \pm i\lambda_0$ with $\lambda_0 = \sqrt{|\kappa|^2 - \delta^2}$ [44]. While in the pseudo- \mathcal{APT} -broken region $|\delta| > |\kappa|$, H_{APT} has two real eigenvalues $\lambda_\pm = \pm\lambda_0$. The spontaneous symmetry breaking occurs at the EP $|\kappa| = |\delta|$, where $\lambda_0 = 0$. In the classical limit, the field operators \hat{a}_1 and \hat{a}_2^\dagger are replaced by complex numbers, and the model reduces to the non-Hermitian system with \mathcal{APT} symmetry [36, 37]. In the quantum realm, we name it as pseudo- \mathcal{APT} symmetry in the sense that H_{APT} is non-Hermitian while \mathcal{H} is Hermitian.

The field operators at time t can be obtained from the dynamical equation (2) as [44]

$$\hat{a}_j(t) = A\hat{a}_j(0) + B\hat{a}_j^\dagger(0), \quad (4)$$

where \bar{j} represents the different mode number from j . In the pseudo- \mathcal{APT} -broken (symmetric) region, we have $A = \cos(\lambda_0 t) - i\frac{\delta}{\lambda_0} \sin(\lambda_0 t)$ ($A = \cosh(\lambda_0 t) -$

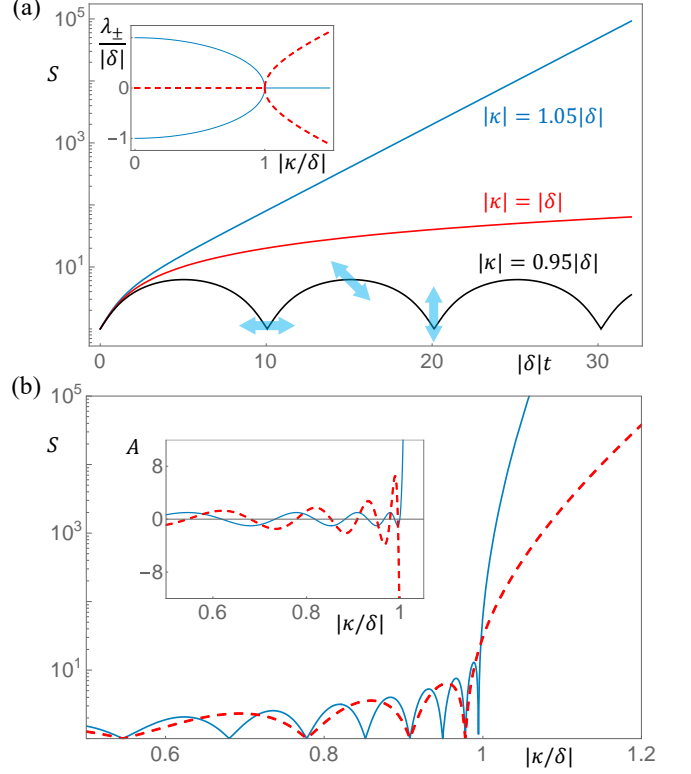


FIG. 1: Pseudo- \mathcal{APT} symmetry induced quantum squeezing dynamics. (a) The squeezing factor versus evolution time for different κ . $|\kappa|/\delta = 0.95, 1$ and 1.05 correspond to pseudo- \mathcal{APT} broken, EP and pseudo- \mathcal{APT} symmetric regions, respectively. Blue arrows indicate the two-mode squeezing directions for $\kappa, \delta > 0$. The inset shows the eigenvalues of H_{APT} . Solid (dashed) lines are the real (imaginary) parts. (b) Squeezing factor versus κ for different evolution time. Solid (dashed) line corresponds to $|\delta|t = 30$ ($|\delta|t = 15$). Inset shows A versus $|\kappa|/\delta$ with $|\delta|t = 30$. Solid (dashed) line is the real (imaginary) part. $B = -\kappa \text{Im}[A]/\delta$.

$i\frac{\delta}{\lambda_0} \sinh(\lambda_0 t)$) and $B = \frac{\kappa}{\lambda_0} \sin(\lambda_0 t)$ ($B = \frac{\kappa}{\lambda_0} \sinh(\lambda_0 t)$). $|A|^2 - |B|^2 = 1$ in both regions and the bosonic commutation relations $[\hat{a}_j(t), \hat{a}_{j'}^\dagger(t)] = [\hat{a}_j(0), \hat{a}_{j'}^\dagger(0)] = \delta_{jj'}$ are preserved without Langevin noises [44].

The two-mode quantum squeezed states are generated from the terms $\hat{a}_1^\dagger \hat{a}_2^\dagger - \hat{a}_1 \hat{a}_2$ in \mathcal{H} and can be characterized by the quadrature operators $\hat{X}_j(\varphi, t) = [e^{-i\varphi} \hat{a}_j(t) + h.c.]/2$ of the two modes, which satisfy $\hat{X}_1(\varphi_+, t) \pm \hat{X}_2(\varphi_+, t) = S^{\pm 1} [\hat{X}_1(\varphi_-, 0) \pm \hat{X}_2(\varphi_-, 0)]$. Here $A = A_0 e^{i\varphi_A}$ and $B = B_0 e^{i\varphi_B}$ with the positive amplitudes $A_0^2 - B_0^2 = 1$, $S = A_0 + B_0 \geq 1$ is the two-mode squeezing factor, $\varphi_+ = (\varphi_B + \varphi_A)/2$ is the squeezing angle. The angle $\varphi_- = (\varphi_B - \varphi_A)/2$ is not important because the initial state is usually unentangled and isotropic (e.g. the vacuum or coherent state).

Fig. 1 shows the transition between different types of quantum squeezing behaviors with the pseudo- \mathcal{APT} symmetry starting from an initial vacuum or coherent

state. In the pseudo- \mathcal{APT} -symmetric region ($|\kappa/\delta| > 1$), one of the eigenmodes disappears after a long time evolution due to purely imaginary λ_{\pm} , therefore $A_0 \simeq B_0 \simeq \frac{\kappa}{2\lambda_0} e^{\lambda_0 t}$ at the long time and $S \simeq \frac{\kappa}{\lambda_0} e^{\lambda_0 t}$ grows exponentially. The squeezing angle ϕ_+ quickly changes from $\frac{1}{2}\text{Arg}[\kappa]$ to its saturated value $\frac{1}{2}\text{Arg}[\kappa\lambda_0 - i\kappa\delta]$. In the pseudo- \mathcal{APT} -broken region, S shows oscillating behavior with a period $T = \pi/\lambda_0$, going back to 1 (non-squeezing) at $t = nT$ and reaching the maximum $S_{\max} = \sqrt{(|\delta| + |\kappa|)/(|\delta| - |\kappa|)}$ at $t = (n + 1/2)T$ (n is an integer). In each period starting from $S = 1$, φ_+ changes from $\frac{1}{2}\text{Arg}[\kappa]$ to $\frac{1}{2}\text{Arg}[-i\kappa\delta]$ as S increases to the maximum, and then to $\frac{1}{2}\text{Arg}[-\kappa]$ as S decreases to 1, as schematically illustrated in Fig. 1a. At the EP, two eigenmodes coalesce to a single mode. We have $A = 1 - i\delta t$, $B = \kappa t$ [44], and $S = \sqrt{1 + \delta^2 t^2} + |\kappa|t$ increases linearly at long time $|\delta|t \gg 1$. φ_+ changes monotonically from $\frac{1}{2}\text{Arg}[\kappa]$ to $\frac{1}{2}\text{Arg}[-i\kappa\delta]$. The results at the EP are consistent with the $|\kappa| \rightarrow |\delta|$ limit from both sides.

Since the squeezing behaviors change dramatically across the EP, the dynamical quantum state at a given time should also be sensitive to the system parameters δ , κ around the EP. In Fig. 1b, we plot S as a function of $|\kappa/\delta|$ at different times. We see S oscillates with increasing amplitude and frequency as $|\kappa|$ is approaching the EP. Near the EP, the squeezing factor (thereby the quantum state) exhibits a sharp change around $S = 1$ (*i.e.*, for κ satisfying $\lambda_0 t = n\pi$), where the system returns to its initial non-squeezing quantum state. The coefficients A and B show similar oscillation behaviors as S (the inset of Fig. 1b). Such critical behavior around the EP can be utilized to implement ultra-precision quantum sensing.

Quantum sensing.—Precision measurements are long pursued due to their vital importance in physics and many other sciences. Quantum sensing, such as large squeezing factor state, quantum entanglement [41, 42], and phase-transition criticality based sensors [54–59], utilize unique quantum phenomena for ultra-precision measurements. Recent studies showed that the EPs of the \mathcal{PT} -symmetry can enhance the optical sensing in the classical region [60]. Here we explore ultra-precision quantum sensing enabled by the quantum pseudo- \mathcal{APT} -symmetry without Langevin noises.

We focus on the pseudo- \mathcal{APT} -broken region $|\kappa| < |\delta|$ (see [44] for discussions on the region $|\kappa| > |\delta|$), which is dynamical stable without the exponential growth of excitations. We propose a simple scheme to measure A and B directly, which are sensitive to the system parameters κ , δ and thus can be used to sense κ and δ . The sensing precision is at the same order as quantum Cramér-Rao bound set by the quantum Fisher information of the quantum state, which shows divergent feature close to the EP.

We consider a coherent initial state $|\psi_0\rangle = |\alpha_1, \alpha_2\rangle$ of two bosonic modes for the quantum sensor. After an evolution time t , we perform the quadrature measurement $\hat{X}_j(0, t)$ of the final states using standard homodyne de-

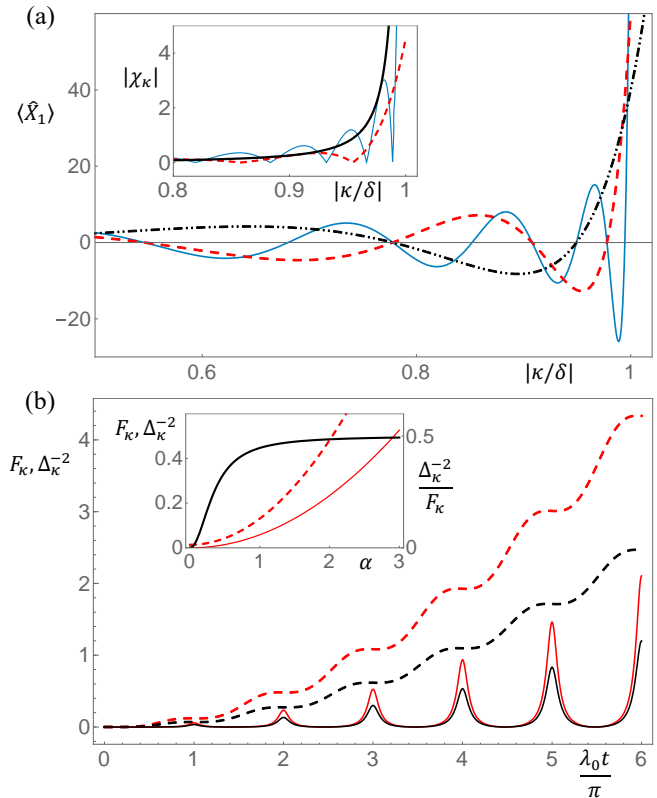


FIG. 2: Quantum sensing based on pseudo- \mathcal{APT} symmetry. (a) The quadrature $\langle \hat{X}_1 \rangle$ versus κ at different evolution time, with $\alpha = 2 \cdot \text{sign}(\delta)$. $|\delta|t = 10, 15$ and 30 are shown by the dash-dotted, dashed and solid lines, respectively. Inset shows the corresponding susceptibility $|\chi_\kappa|$ (in unit of 10^3), with bold solid line showing the results with κ -dependent time satisfying $\lambda_0 t = 2\pi$. The working points are located near $\langle \hat{X}_1 \rangle = 0$ (*i.e.*, the maxima of χ_κ). (b) The inverse variance Δ_κ^{-2} (solid lines) of the observable and the quantum Fisher information F_κ (dashed lines) as functions of evolution times (in unit of 10^7) with $\alpha = 2$. Red and black lines are for $\kappa/\delta = 0.95$ and 0.94 , respectively. Local maxima of Δ_κ^{-2} give the work points $\lambda_0 t = n\pi$. Inset shows the results as functions of α for $\lambda_0 t = 2\pi$ and $\kappa/\delta = 0.95$, with bold black line corresponding to $\Delta_\kappa^{-2}/F_\kappa$.

tection [61], which give the mean value and variance

$$\langle \hat{X}_j(0, t) \rangle_{\psi_0} = \text{Re}[A\alpha_j + B\alpha_j^*] \quad (5)$$

$$[\Delta \hat{X}_j(0, t)]^2 = \frac{1}{4}(A_0^2 + B_0^2), \quad (6)$$

with $\bar{j} \neq j$. Therefore we can determine A and B from the measurement results for the estimation of κ or δ . Without loss of generality, we choose $\kappa\delta > 0$ and set $\alpha_2 = -i\alpha_1 \equiv \alpha$ (different choices of parameters α_i give similar results, which do not affect the sensing precision). In Fig. 2a, we plot the observable $\langle \hat{X}_1(0, t) \rangle_{\psi_0} = \alpha \sin(\lambda_0 t) \frac{\kappa + \delta}{\lambda_0}$ as a function of κ with fixed δ and t , which possesses strong and fast oscillation close to the EP. Such oscillation becomes more pronounced as the evolution time increases.

The measurement of the change of $\langle \hat{X}_j(0, t) \rangle_{\psi_0}$ with κ gives the susceptibility $\chi_\kappa(t) \equiv \partial_\kappa \langle \hat{X}_1(0, t) \rangle_{\psi_0}$ which exhibits divergent feature close to the EP $\kappa \rightarrow \delta$ (*i.e.*, $\lambda_0 \rightarrow 0$). Similar results apply to the susceptibility with δ . In Fig. 2a, we plot χ_κ for a fixed evolution time as well as the sensor working point $t = nT$. The later one possesses a divergent scaling $\chi_\kappa(nT) = -\alpha \frac{\kappa(\kappa+\delta)n\pi}{\lambda_0^3} \sim \lambda_0^{-3}$. Longer evolution time is required for smaller λ_0 to observe such divergence. Note that the eigenvalues of H_{APT} have a square-root splitting with divergent sensitivity $\partial_\kappa \lambda_0 = -\frac{\kappa}{\lambda_0}$ close to the EP. In addition, the eigenmodes are not orthogonal and coalesce at the EP, which are responsible for the factor λ_0^{-1} in the final Bosonic field $\hat{a}_j(t)$. Together they give the divergent scaling $\chi_\kappa(t) \sim \lambda_0^{-3}$ for an evolution time $t \sim \lambda_0^{-1}$.

The precision of the parameter estimation of κ is given by the variance $\Delta_\kappa^2 = [\Delta \hat{X}_1]^2 / \chi_\kappa^2$, and the performance of the sensing scheme can be evaluated by comparing the inverse variance Δ_κ^{-2} with the quantum Fisher information F_κ , whose inverse gives the ultimate precision for quantum sensing, *i.e.*, reaching quantum Cramér-Rao bound $\Delta_\kappa^{-2} \leq F_\kappa$ (optimal measurement is usually required). For the coherent initial state $|\psi_0\rangle$,

$$F_\kappa(t) = 4A_0^4 \left| \partial_\kappa \frac{B}{A^*} \right|^2 + 4(A_0^2 + B_0^2) \sum_j |\partial_\kappa \langle \hat{a}_j(t) \rangle_{\psi_0}|^2 - 16\Re[A^* B^* \partial_\kappa \langle \hat{a}_1(t) \rangle_{\psi_0} \partial_\kappa \langle \hat{a}_2(t) \rangle_{\psi_0}] \quad (7)$$

after the evolution time t [44]. In Fig. 2b, we compare Δ_κ^{-2} with F_κ at different evolution times. We see that Δ_κ^{-2} has some narrow peaks when κ satisfies $t = nT$ (*i.e.*, the variance Δ_κ reaches the minimum) for fixed δ and $|\kappa| \lesssim |\delta|$, while $F_\kappa(t)$ smoothly increases with κ and takes larger values for all κ near the EP. At working points $t = nT$, $F_\kappa(nT) = \left[8 + \frac{4\kappa^2}{\alpha^2(\kappa+\delta)^2} \right] \chi_\kappa^2 \sim \lambda_0^{-6}$, while $\Delta_\kappa^{-2}(nT) = 4\chi_\kappa^2 \simeq 0.5F_\kappa$ for coherent amplitudes α that are not too weak (*e.g.*, $\alpha \sim 2$), as shown in Fig. 2b. During the evolution, the number of bosonic excitations $N \sim \lambda_0^{-2}$, therefore $\Delta_\kappa^{-2} \sim N^2 t^2$, which is at the same order as the Heisenberg limit.

Notice that at the working points $t = nT$, the squeezing factor $S = 1$, therefore the ultra-precision sensitivity originates from the pseudo- \mathcal{APT} symmetry breaking, making our scheme distinct from traditional quantum sensors based on large squeezing factors.

Experimental realization.—The quantum pseudo- \mathcal{APT} symmetry physics can be realized in quantum optics systems or atomic BECs. In the quantum optics implementation, we can utilize nonlinear wave mixing such as spontaneous parametric down conversion (SPDC) [62, 63] and spontaneous four-wave mixing (SFWM) [64, 65] with carefully designed parameters. A schematic illustration of the optical setup is shown in Fig. 3a and more detailed studies are provided in [44]. In SFWM, two quantum modes ($\hat{a}_{1,2}$) copropagate along the z direction in

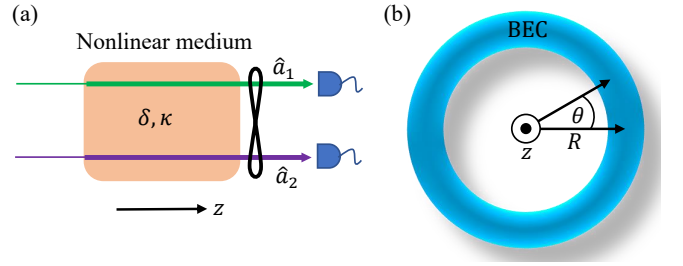


FIG. 3: Experimental implementations. (a) Schematic optical setup for realizing pseudo- \mathcal{APT} symmetry physics through nonlinear spontaneous four-wave mixing. (b) Experimental realization based on a cold atomic BEC in a ring trap.

the nonlinear optical medium and are coupled through a nonlinear coupling coefficient κ which can be tuned by changing two additional pump lasers' intensity and frequency, as well as the material properties. The parameter δ is associated with the phase mismatching $\delta = -\Delta k/2$ depending on laser frequency and propagation direction, where $\Delta k = (\mathbf{k}_1 + \mathbf{k}_2 - \sum \mathbf{k}_{\text{pump}}) \cdot \hat{\mathbf{z}}$ with \mathbf{k}_j being the wave vectors and $\hat{\mathbf{z}}$ the unit vector. In this system, the propagation along the z direction simulates the time evolution in our theoretical model (*i.e.*, $t = z$). In the quantum sensing, the final output quantum fields of two modes from the nonlinear medium will be measured using standard homodyne detection, yielding the mean value and variance of quadratures of two modes.

In the atomic implementation, we consider a BEC in a ring dipole trap (as shown in Fig. 3b) with a strong confinement along z and radial directions, which can be realized by Laguerre-Gaussian lasers as demonstrated in recent experiments [66, 67]. The dynamics are reduced to one dimension (*i.e.*, the azimuthal angle θ). We can expand the BEC field operator in the angular momentum space as [68, 69]

$$\hat{\Psi}(\theta, t) = e^{-i\mu t - i\pi/4} \Phi(t) + e^{-i\mu t} \sum_{n \neq 0} \hat{\psi}_n(t) \frac{e^{in\theta}}{\sqrt{2\pi}}, \quad (8)$$

where Φ is the condensate wave function (Φ is real initially and $\pi/4$ is a gauge choice), $\mu = -g|\Phi|^2 - g \sum_n \langle \hat{\psi}_n^\dagger \hat{\psi}_n \rangle / 2\pi$ is the chemical potential, and g is the interaction strength ($g > 0$ corresponds to attractive interaction). The quantum excitation operators $\hat{\psi}_n(t)$ satisfy the Bogoliubov equation [44]

$$i\partial_t \begin{pmatrix} \hat{\psi}_n \\ \hat{\psi}_{-n}^\dagger \end{pmatrix} = \begin{pmatrix} \delta_n & i\kappa \\ i\kappa^* & -\delta_n \end{pmatrix} \begin{pmatrix} \hat{\psi}_n \\ \hat{\psi}_{-n}^\dagger \end{pmatrix}, \quad (9)$$

which shares the same form as Eq. 2. Here $\delta_n = n^2 E_1 - g|\Phi|^2$, $\kappa = g\Phi^2$, and $E_1 = \frac{1}{2mR^2}$ is the kinetic energy of the first excited state along the ring with radius R . At $g = 0$, the quantum pseudo- \mathcal{APT} symmetry is broken for all n . As g increases, the BEC becomes dynamical unstable when $2g|\Phi|^2 > E_1$ (*i.e.*, $|\kappa| > |\delta_1|$),

where the pseudo- \mathcal{APT} symmetry is restored for $n = 1$, and the excitation number and squeezing factor grow exponentially [70, 71]. For the quantum sensing, we can first prepare the BEC to its ground state with $g \simeq 0$. The initial coherent state for $n = \pm 1$ can be generated by Raman process with Laguerre-Gaussian beams carrying ± 1 orbital angular momentum. Then we increase g to the working point near the EP (*i.e.*, $2g|\Phi|^2 = E_1$). The quadratures \hat{X}_n , which is proportional to the visibility of the density modulation along θ , can be measured by density imaging. The performance of the sensor is very similar as that shown in Fig. 2 [44]. We want to point out that the Kerr interaction of photons as well as the interaction between excitations of the BEC are extremely weak, which can hardly affect the finite duration dynamics of interest [44].

Conclusion.—In summary, we construct a quantum pseudo- \mathcal{APT} symmetry without Langevin noises and show that its transition across EP yields a dramatic change of quantum squeezed dynamics. The divergent sensitivity of squeezed states close to the EP can be utilized for ultra-precision sensing approaching the quantum limit. The experimental realization of such quantum pseudo- \mathcal{APT} symmetry in nonlinear quantum optical wave mixing and ultracold atomic BECs will provide realistic platforms for studying quantum non-Hermitian physics and its quantum sensing applications. The two-mode quantum pseudo- \mathcal{APT} symmetry can also be generalized to a multi-mode system supporting higher-order EPs [72, 73], which may lead to novel symmetry breaking physics and even higher sensing precision.

Acknowledgments.—X.W.L. and C.Z. acknowledge support from NSF (PHY-2110212), ARO (W911NF17-1-0128), and AFOSR (FA9550-20-1-0220,FA9550-22-1-0043). S.D. acknowledges support from DOE (DE-SC0022069).

* Electronic address: Chuanwei.Zhang@utdallas.edu

† Electronic address: dusw@utdallas.edu

- [1] C. M. Bender and S. Boettcher, Real Spectra in Non-Hermitian Hamiltonians Having \mathcal{PT} Symmetry, *Phys. Rev. Lett.* **80**, 5243 (1998).
- [2] C. M. Bender, Making sense of non-Hermitian Hamiltonians, *Rep. Prog. Phys.* **70**, 947 (2007).
- [3] R. El-Ganainy, K. G. Makris, M. Khajavikhan, Z. H. Musslimani, S. Rotter, and D. N. Christodoulides, Non-Hermitian physics and \mathcal{PT} symmetry, *Nat. Phys.* **14**, 11 (2018).
- [4] Ş. K. Özdemir, S. Rotter, F. Nori, and L. Yang, Parity-time symmetry and exceptional points in photonics, *Nat. Mater.* **18**, 783 (2019).
- [5] M.-A. Miri and A. Alù, Exceptional points in optics and photonics, *Science* **363**, 1457 (2019).
- [6] V. V. Konotop, J. Yang, and D. A. Zezyulin, Nonlinear waves in \mathcal{PT} -symmetric systems, *Rev. Mod. Phys.* **88**, 035002 (2016).
- [7] L. Feng, R. El-Ganainy and L. Ge, Non-Hermitian photonics based on parity-time symmetry, *Nat. Photonics* **11**, 752 (2017).
- [8] R. El-Ganainy, K. G. Makris, D. N. Christodoulides, and Z. H. Musslimani, Theory of coupled optical \mathcal{PT} -symmetric structures, *Opt. Lett.* **32**, 2632 (2007).
- [9] A. Guo, G. J. Salamo, D. Duchesne, R. Morandotti, M. Volatier-Ravat, V. Aimez, G. A. Siviloglou, and D. N. Christodoulides, Observation of \mathcal{PT} -Symmetry Breaking in Complex Optical Potentials, *Phys. Rev. Lett.* **103**, 093902 (2009).
- [10] C. E. Rüter, K. G. Makris, R. El-Ganainy, D. N. Christodoulides, M. Segev, and D. Kip, Observation of parity-time symmetry in optics, *Nat. Phys.* **6**, 192 (2010).
- [11] B. Peng, Ş. K. Özdemir, F. Lei, F. Monifi, M. Gianfreda, G. L. Long, S. Fan, F. Nori, C. M. Bender, and L. Yang, Parity-time-symmetric whispering-gallery microcavities, *Nat. Phys.* **10**, 394 (2014).
- [12] C. Hang, G. Huang, and V. V. Konotop, \mathcal{PT} Symmetry with a System of Three-Level Atoms, *Phys. Rev. Lett.* **110**, 083604 (2013).
- [13] Z. Zhang, Y. Zhang, J. Sheng, L. Yang, M.-A. Miri, D. N. Christodoulides, B. He, Y. Zhang, and M. Xiao, Observation of Parity-Time Symmetry in Optically Induced Atomic Lattices, *Phys. Rev. Lett.* **117**, 123601 (2016).
- [14] J. Schindler, A. Li, M. C. Zheng, F. M. Ellis, and T. Kottos, Experimental study of active LRC circuits with \mathcal{PT} symmetries, *Phys. Rev. A* **84**, 040101 (2011).
- [15] R. Fleury, D. Sounas, and A. Alù, An invisible acoustic sensor based on parity-time symmetry, *Nat. Commun.* **6**, 5905 (2015).
- [16] X. Zhu, H. Ramezani, C. Shi, J. Zhu, and X. Zhang, \mathcal{PT} -Symmetric Acoustics, *Phys. Rev. X* **4**, 031042 (2014).
- [17] L. Feng, Z. J. Wong, R.-M. Ma, Y. Wang, and X. Zhang, Single-mode laser by parity-time symmetry breaking, *Science* **346**, 972 (2014).
- [18] H. Hodaei, M.-A. Miri, M. Heinrich, D. N. Christodoulides, and M. Khajavikhan, Parity-time-symmetric microring lasers, *Science* **346**, 975 (2014).
- [19] J. Wiersig, Enhancing the Sensitivity of Frequency and Energy Splitting Detection by Using Exceptional Points: Application to Microcavity Sensors for Single-Particle Detection, *Phys. Rev. Lett.* **112**, 203901 (2014).
- [20] Z.-P. Liu, J. Zhang, Ş. K. Özdemir, B. Peng, H. Jing, X.-Y. Lü, C.-W. Li, L. Yang, F. Nori, and Y.-X. Liu, Metrology with \mathcal{PT} -Symmetric Cavities: Enhanced Sensitivity near the \mathcal{PT} -Phase Transition, *Phys. Rev. Lett.* **117**, 110802 (2016).
- [21] Y. Choi, C. Hahn, J. W. Yoon, S. H. Song, and P. Berini, Extremely broadband, on-chip optical nonreciprocity enabled by mimicking nonlinear anti-adiabatic quantum jumps near exceptional points, *Nat. Commun.* **8**, 14154 (2017).
- [22] H.-K. Lau and A. A. Clerk, Fundamental limits and non-reciprocal approaches in non-Hermitian quantum sensing, *Nat. Commun.* **9**, 4320 (2018).
- [23] M. Zhang, W. Sweeney, C. W. Hsu, L. Yang, A. D. Stone, and L. Jiang, Quantum Noise Theory of Exceptional Point Amplifying Sensors, *Phys. Rev. Lett.* **123**, 180501 (2019).
- [24] Y. Chu, Y. Liu, H. Liu, and J. Cai, Quantum Sens-

- ing with a Single-Qubit Pseudo-Hermitian System, *Phys. Rev. Lett.* **124**, 020501 (2020).
- [25] M. Naghiloo, M. Abbasi, Y. N. Joglekar, and K. W. Murch, Quantum state tomography across the exceptional point in a single dissipative qubit, *Nat. Phys.* **15**, 1232 (2019).
- [26] Y. Wu, et al. Observation of parity-time symmetry breaking in a single-spin system, *Science* **364**, 878 (2019).
- [27] Yu, S. et al. Experimental Investigation of Quantum PT-Enhanced Sensor. *Phys. Rev. Lett.* **125**, 240506 (2020).
- [28] S. Scheel and A. Szameit, PT-symmetric photonic quantum systems with gain and loss do not exist, *Europhysics Lett.* **122**, 34001 (2018).
- [29] L. Ge and H. E. Türeci, Antisymmetric \mathcal{PT} -photonic structures with balanced positive- and negative-index materials, *Phys. Rev. A* **88**, 053810 (2013).
- [30] P. Peng, W. Cao, C. Shen, W. Qu, J. Wen, L. Jiang, and Y. Xiao, Anti-parity-time symmetry with flying atoms, *Nat. Phys.* **12**, 1139 (2016).
- [31] J.-H. Wu, M. Artoni, and G. C. La Rocca, Non-Hermitian Degeneracies and Unidirectional Reflectionless Atomic Lattices, *Phys. Rev. Lett.* **113**, 123004 (2014).
- [32] F. Yang, Y.-C. Liu, and L. You, Anti- \mathcal{PT} symmetry in dissipatively coupled optical systems, *Phys. Rev. A* **96**, 053845 (2017).
- [33] V. V. Konotop and D. A. Zezyulin, Odd-Time Reversal \mathcal{PT} Symmetry Induced by an Anti- \mathcal{PT} -Symmetric Medium, *Phys. Rev. Lett.* **120**, 123902 (2018).
- [34] X.-L. Zhang, S. Wang, B. Hou, and C. T. Chan, Dynamically Encircling Exceptional Points: In situ Control of Encircling Loops and the Role of the Starting Point, *Phys. Rev. X* **8**, 021066 (2018).
- [35] Y. Li, Y.-G. Peng, L. Han, M.-A. Miri, W. Li, M. Xiao, X.-F. Zhu, J. Zhao, A. Alù, S. Fan, and C.-W. Qiu, Anti-parity-time symmetry in diffusive systems, *Science* **364**, 170 (2018).
- [36] Y. Jiang, Y. Mei, Y. Zuo, Y. Zhai, Jensen Li, J. Wen, and S. Du, Anti-Parity-Time Symmetric Optical Four-Wave Mixing in Cold Atoms, *Phys. Rev. Lett.* **123**, 193604 (2019).
- [37] M.-A. Miri and A. Alù, Nonlinearity-induced PT-symmetry without material gain, *New J. Phys.* **18**, 065001 (2016).
- [38] Y.-X. Wang and A. A. Clerk, Non-Hermitian dynamics without dissipation in quantum systems, *Phys. Rev. A* **99**, 063834 (2019).
- [39] S. L. Braunstein and P. van Loock, Quantum information with continuous variables, *Rev. Mod. Phys.* **77**, 513 (2005).
- [40] A. I. Lvovsky, Squeezed light, *Photon. Sci. Found., Technol. Appl.* **1**, 121 (2015).
- [41] V. Giovannetti, S. Lloyd, and L. Maccone, Advances in quantum metrology, *Nat. Photon.* **5**, 222 (2011).
- [42] L. Pezzè, A. Smerzi, M. K. Oberthaler, R. Schmied, and P. Treutlein, Quantum metrology with nonclassical states of atomic ensembles, *Rev. Mod. Phys.* **90**, 035005 (2018).
- [43] H. Smith and C. J. Pethick, Bose-Einstein Condensation in Dilute Gases, Cambridge University Press, (2001).
- [44] See Supplementary Materials for more information about the squeezing properties, quantum Fisher information, implementation with quantum optics and BEC, and Kerr nonlinearity with Refs. [45–53].
- [45] N. Bartolo, F. Minganti, W. Casteels, and C. Ciuti, Exact steady state of a Kerr resonator with one- and two-photon driving and dissipation: Controllable Wigner-function multimodality and dissipative phase transitions, *Phys. Rev. A* **94**, 033841 (2016).
- [46] P. Krantz, A. Bengtsson, M. Simoen, S. Gustavsson, V. Shumeiko, W. D. Oliver, C. M. Wilson, P. Delsing, and J. Bylander, Single-shot read-out of a superconducting qubit using a Josephson parametric oscillator, *Nat. Commun.* **7**, 11417 (2016).
- [47] F. Minganti, A. Biella, N. Bartolo, and C. Ciuti, Spectral theory of Liouvillians for dissipative phase transitions, *Phys. Rev. A* **98**, 042118 (2018).
- [48] T. L. Heugel, M. Biondi, O. Zilberberg, and R. Chitra, Quantum Transducer Using a Parametric Driven-Dissipative Phase Transition, *Phys. Rev. Lett.* **123**, 173601 (2019).
- [49] S. Lieu, R. Belyansky, J. T. Young, R. Lundgren, V. V. Albert, and A. V. Gorshkov, Symmetry Breaking and Error Correction in Open Quantum Systems, *Phys. Rev. Lett.* **125**, 240405 (2020).
- [50] Xin H. H. Zhang and Harold U. Baranger, Driven-dissipative phase transition in a Kerr oscillator: From semiclassical \mathcal{PT} symmetry to quantum fluctuations, *Phys. Rev. A* **103**, 033711 (2021).
- [51] R. Di Candia, F. Minganti, K. V. Petrovnin, G. S. Paraoanu, and S. Felicetti, Critical parametric quantum sensing, [arXiv:2107.04503](https://arxiv.org/abs/2107.04503).
- [52] D. G. Fried, T. C. Killian, L. Willmann, D. Landhuis, S. C. Moss, D. Kleppner, and T. J. Greytak, Bose-Einstein Condensation of Atomic Hydrogen, *Phys. Rev. Lett.* **81**, 3811 (1998).
- [53] N. P. Robins, P. A. Altin, J. E. Debs, and J. D. Close, Atom lasers: Production, properties and prospects for precision inertial measurement, *Phys. Rep.* **529**, 265 (2013).
- [54] M. Tsang, Quantum transition-edge detectors, *Phys. Rev. A* **88**, 021801 (2013).
- [55] M. Skotiniotis, P. Sekatski, and W. Dür, Quantum metrology for the Ising Hamiltonian with transverse magnetic field, *New J. Phys.* **17**, 073032 (2015).
- [56] K. Macieszczak, M. Guță, I. Lesanovsky, and J. P. Garrahan, Dynamical phase transitions as a resource for quantum enhanced metrology, *Phys. Rev. A* **93**, 022103 (2016).
- [57] Y. Chu, S. Zhang, B. Yu, and J. Cai, Dynamic Framework for Criticality-Enhanced Quantum Sensing, *Phys. Rev. Lett.* **126**, 010502 (2021).
- [58] L. Garbe, M. Bina, A. Keller, M. G. A. Paris, and S. Felicetti, Critical Quantum Metrology with a Finite-Component Quantum Phase Transition, *Phys. Rev. Lett.* **124**, 120504 (2020).
- [59] M. M. Rams, P. Sierant, O. Dutta, P. Horodecki, and J. Zakrzewski, At the Limits of Criticality-Based Quantum Metrology: Apparent Super-Heisenberg Scaling Revisited, *Phys. Rev. X* **8**, 021022 (2018).
- [60] J. Wiersig, Review of exceptional point-based sensors, *Photon. Res.* **8**, 1457 (2020).
- [61] H. M. Wiseman and G. J. Milburn, Quantum Measurement and Control (Cambridge University Press, Cambridge, 2010).
- [62] S. E. Harris, M. K. Oshman, and R. L. Byer, Observation of Tunable Optical Parametric Fluorescence, *Phys. Rev. Lett.* **18**, 732 (1967).
- [63] D. N. Klyshko, A. N. Penin, and B. F. Polkovnikov, Parametric Luminescence and Light Scattering by Polaritons,

- JETP Lett. **11**, 05 (1970).
- [64] S. Du, J. Wen, and M. H. Rubin, Narrowband biphoton generation near atomic resonance, *J. Opt. Soc. Am. B* **25**, C98 (2008).
- [65] L. Zhao, Y. Su, and S. Du, Narrowband biphoton generation in the group delay regime, *Phys. Rev. A* **93**, 033815 (2016).
- [66] O. Morizot, Y. Colombe, V. Lorent, H. Perrin, and B. M. Garraway, Ring trap for ultracold atoms, *Phys. Rev. A* **74**, 023617 (2006).
- [67] S. Eckel, J. G. Lee, F. Jendrzejewski, N. Murray, C. W. Clark, C. J. Lobb, W. D. Phillips, M. Edwards, and G. K. Campbell, Hysteresis in a quantized superfluid atomic circuit, *Nature* **506**, 200 (2014).
- [68] A. Griffin, Conserving and gapless approximations for an inhomogeneous Bose gas at finite temperatures, *Phys. Rev. B* **53**, 9341 (1996).
- [69] R. Ozeri, N. Katz, J. Steinhauer, and N. Davidson, Colloquium: Bulk Bogoliubov excitations in a Bose-Einstein condensate, *Rev. Mod. Phys.* **77**, 187 (2005).
- [70] V. A. Yurovsky, Quantum effects on dynamics of instabilities in Bose-Einstein condensates, *Phys. Rev. A* **65**, 033605 (2002).
- [71] E. A. Calzetta and B. L. Hu, Bose-Einstein condensate collapse and dynamical squeezing of vacuum fluctuations, *Phys. Rev. A* **68**, 043625 (2003).
- [72] H. Hodaei, A. U. Hassan, S. Wittek, H. Garcia-Gracia, R. El-Ganainy, D. N. Christodoulides, and M. Khajavikhan, Enhanced sensitivity at higher-order exceptional points, *Nature* **548**, 187 (2017).
- [73] S. Wang, B. Hou, W. Lu, Y. Chen, Z. Q. Zhang, and C. T. Chan, Arbitrary order exceptional point induced by photonic spin-orbit interaction in coupled resonators, *Nat. Commun.* **10**, 832 (2019).

SUPPLEMENTARY MATERIALS

S1. Derivation of the dynamical equation

As we discussed in the main text, the \mathcal{APT} -symmetric dynamical equation is obtained from a second-quantized Hamiltonian which is Hermitian, with pair generation of particles. The second-quantized Hamiltonian reads

$$\mathcal{H} = \delta \left[\hat{a}_1^\dagger \hat{a}_1 + \hat{a}_2^\dagger \hat{a}_2 \right] + i\kappa \left[\hat{a}_1^\dagger \hat{a}_2^\dagger - \hat{a}_1 \hat{a}_2 \right]. \quad (\text{S1})$$

The dynamical equation can be obtained from the Heisenberg equation (we set $\hbar = 1$)

$$\begin{aligned} i\partial_t \hat{a}_j &= [\hat{a}_j, \mathcal{H}] \\ i\partial_t \hat{a}_j^\dagger &= [\hat{a}_j^\dagger, \mathcal{H}]. \end{aligned} \quad (\text{S2})$$

Using the commutation relations $[\hat{a}_j, \hat{a}_{j'}^\dagger] = \delta_{j,j'}$ and $[\hat{a}_j, \hat{a}_{j'}] = 0$, it is straightforward to show that

$$\begin{aligned} i\partial_t \hat{a}_1 &= \delta \hat{a}_1 + i\kappa \hat{a}_2^\dagger \\ i\partial_t \hat{a}_2^\dagger &= i\kappa \hat{a}_1 - \delta \hat{a}_2^\dagger. \end{aligned} \quad (\text{S3})$$

Thus we obtain the dynamical equation

$$i\partial_t \left(\hat{a}_1, \hat{a}_2^\dagger \right)^T = H_{APT} \left(\hat{a}_1, \hat{a}_2^\dagger \right)^T, \quad (\text{S4})$$

with the non-Hermitian dynamical Hamiltonian matrix given by

$$H_{APT} = \delta \sigma_z + i\kappa \sigma_x = \begin{pmatrix} \delta & i\kappa \\ i\kappa & -\delta \end{pmatrix}. \quad (\text{S5})$$

It is easy to show that the dynamical Hamiltonian possesses \mathcal{APT} -symmetry with the anticommutation relation $\mathcal{PT}H_{APT} = -H_{APT}\mathcal{PT}$, where parity operator $\mathcal{P} = \sigma_x$ and time-reversal operator $\mathcal{T} = \mathcal{K}$ the complex conjugate. We want to point out that the \mathcal{APT} -symmetric Hamiltonian can be written as $H_{APT} = iH_{PT}$ with $H_{PT} = -i\delta\sigma_z + \kappa\sigma_x$ satisfying the \mathcal{PT} -symmetry $\mathcal{PT}H_{PT} = H_{PT}\mathcal{PT}$.

The above discussion is gauge independent. This can be shown by considering a different gauge choice, where we replace \hat{a}_2 by $i\hat{a}_2$ (i.e., \hat{a}_2^\dagger by $-i\hat{a}_2^\dagger$). The second-quantized Hamiltonian now reads

$$\mathcal{H} = \delta \left[\hat{a}_1^\dagger \hat{a}_1 + \hat{a}_2^\dagger \hat{a}_2 \right] + \kappa \left[\hat{a}_1^\dagger \hat{a}_2^\dagger + \hat{a}_1 \hat{a}_2 \right]. \quad (\text{S6})$$

Using the Heisenberg equation $i\partial_t \hat{a}_j = [\hat{a}_j, \mathcal{H}]$ and commutation relations, we obtain

$$\begin{aligned} i\partial_t \hat{a}_1 &= \delta \hat{a}_1 + \kappa \hat{a}_2^\dagger \\ i\partial_t \hat{a}_2^\dagger &= -\kappa \hat{a}_1 - \delta \hat{a}_2^\dagger. \end{aligned} \quad (\text{S7})$$

The dynamical Hamiltonian in $i\partial_t(\hat{a}_1, \hat{a}_2^\dagger)^T = H_{APT}(\hat{a}_1, \hat{a}_2^\dagger)^T$ becomes

$$H_{APT} = \delta\sigma_z + i\kappa\sigma_y = \begin{pmatrix} \delta & \kappa \\ -\kappa & -\delta \end{pmatrix}, \quad (\text{S8})$$

which also possesses the \mathcal{APT} -symmetry $\mathcal{PT}H_{APT} = -H_{APT}\mathcal{PT}$, with $\mathcal{T}H_{APT} = H_{APT}\mathcal{T}$ and $\mathcal{P}H_{APT} = -H_{APT}\mathcal{P}$. We can again write the Hamiltonian as $H_{APT} = iH_{PT}$ with $H_{PT} = -i\delta\sigma_z + \kappa\sigma_y$ satisfying the \mathcal{PT} -symmetry $\mathcal{PT}H_{PT} = H_{PT}\mathcal{PT}$, with $\mathcal{T}H_{PT} = -H_{PT}\mathcal{T}$ and $\mathcal{P}H_{PT} = -H_{PT}\mathcal{P}$.

S2. \mathcal{APT} symmetry, EP and Two-mode squeezing

Consider a general non-Hermitian Hamiltonian matrix H , which satisfies the \mathcal{APT} symmetry $\{\mathcal{PT}, H\} = 0$. We define $|R\rangle$ to be the eigenstate of H with $H|R\rangle = E|R\rangle$ and E the eigenvalue. We thus have $H\mathcal{PT}|R\rangle = -\mathcal{PT}H|R\rangle = -E^*\mathcal{PT}|R\rangle$. In the \mathcal{APT} -symmetric phase, the state $|R\rangle$ possesses \mathcal{PT} symmetry $\mathcal{PT}|R\rangle = |R\rangle$, and we have $H\mathcal{PT}|R\rangle = H|R\rangle = E|R\rangle$. Therefore, we have $E = -E^*$ in the \mathcal{APT} -symmetric phase, which must be purely imaginary. In the \mathcal{APT} -broken phase, the two eigenstates are different $\mathcal{PT}|R\rangle \neq |R\rangle$, and we have a pair of eigenvalues $(E, -E^*)$, which are purely real up to a constant shift. Similar to the \mathcal{PT} symmetry, the \mathcal{APT} symmetry breaking point also gives the EP which corresponds to the change of eigenenergies from purely imaginary to purely real.

The \mathcal{APT} -symmetric matrix H_{APT} in Eq. S5 is non-Hermitian, thus has biorthogonal left and right eigenstates, $H_{APT}|R_\pm\rangle = \lambda_\pm|R_\pm\rangle$ and $H_{APT}^\dagger|L_\pm\rangle = \lambda_\pm^*|L_\pm\rangle$. In the pseudo- \mathcal{APT} -broken region $|\kappa| < |\delta|$, the eigenvalues $\lambda_\pm = \pm\sqrt{\delta^2 - \kappa^2}$, with eigenstates $|R_\pm\rangle = \frac{i\kappa}{2\lambda_\pm}(\frac{\delta \pm \sqrt{\delta^2 - \kappa^2}}{i\kappa}, 1)^T$, and $|L_\pm\rangle = (1, \frac{\delta \mp \sqrt{\delta^2 - \kappa^2}}{i\kappa})^T$. In the pseudo- \mathcal{APT} -symmetric region $|\kappa| > |\delta|$, $\lambda_\pm = \pm i\sqrt{\kappa^2 - \delta^2}$ with $|R_\pm\rangle = \frac{i\kappa}{2\lambda_\pm}(\frac{\delta \pm i\sqrt{\kappa^2 - \delta^2}}{i\kappa}, 1)^T$, and $|L_\pm\rangle = (1, \frac{\delta \pm i\sqrt{\kappa^2 - \delta^2}}{i\kappa})^T$. We have two eigenmodes $\hat{b}_+ \propto \langle L_+|\vec{a}\rangle$ and $\hat{b}_- \propto \langle L_-|\vec{a}\rangle$ with $|\vec{a}\rangle = (\hat{a}_1, \hat{a}_2^\dagger)^T$. We project the operators onto the eigenmodes, then the field operators at time t become

$$\begin{pmatrix} \hat{a}_1(t) \\ \hat{a}_2^\dagger(t) \end{pmatrix} = \begin{pmatrix} A & B \\ B^* & A^* \end{pmatrix} \begin{pmatrix} \hat{a}_1(0) \\ \hat{a}_2^\dagger(0) \end{pmatrix} \quad (\text{S9})$$

with the transfer matrix

$$\begin{pmatrix} A & B \\ B^* & A^* \end{pmatrix} = \sum_{s=\pm} |R_s\rangle e^{-i\lambda_s t} \langle L_s|, \quad (\text{S10})$$

where

$$A = \sum_{s=\pm} \frac{(\lambda_s - \delta)e^{i\lambda_s t}}{2\lambda_s} \quad (\text{S11})$$

$$B = \sum_{s=\pm} \frac{\kappa e^{i\lambda_s t}}{2i\lambda_s}. \quad (\text{S12})$$

At the EP $\kappa = \pm\delta$, the two eigenmodes coalesce to a single mode $\sim \hat{a}_1 \pm i\hat{a}_2^\dagger$, which satisfies $i\partial_t[\hat{a}_1(t) \pm i\hat{a}_2^\dagger(t)] = 2\delta[\hat{a}_1(0) \mp i\hat{a}_2^\dagger(0)]$ and depends on its time-independent orthogonal mode $\sim \hat{a}_1 \mp i\hat{a}_2^\dagger$. Therefore, we have the solution $A = 1 - i\delta t$, $B = \kappa t$. We can define the quadrature operators $\hat{X}_j(\varphi, t) = [e^{-i\varphi}\hat{a}_j(t) + h.c.]/2$ and $\hat{P}_j(\varphi, t) = [e^{-i\varphi}\hat{a}_j(t) - h.c.]/2i$. It can be shown that $\hat{X}_1(\varphi_+, t) \pm \hat{X}_2(\varphi_+, t) = S^{\pm 1}[\hat{X}_1(\varphi_-, 0) \pm \hat{X}_2(\varphi_-, 0)]$ and $\hat{P}_1(\varphi_+, t) \mp \hat{P}_2(\varphi_+, t) = S^{\pm 1}[\hat{P}_1(\varphi_-, 0) \mp \hat{P}_2(\varphi_-, 0)]$, with the squeezing factor $S = A_0 + B_0 \geq 1$ (with $A_0 = |A|, B_0 = |B|$) and the angles $\varphi_\pm = (\text{Arg}[B] \pm \text{Arg}[A])/2$. The oscillation behavior of S (as well as A and B) in the pseudo- \mathcal{APT} -broken region is due to the interference between two eigenmodes.

It can be easily shown that the solutions $\hat{a}_1(t), \hat{a}_2(t)$ satisfy the Bosonic commutation relation. Since the corresponding second-quantized Hamiltonian $\mathcal{H} = \delta[\hat{a}_1^\dagger\hat{a}_1 + \hat{a}_2^\dagger\hat{a}_2] + i\kappa[\hat{a}_1^\dagger\hat{a}_2^\dagger - \hat{a}_1\hat{a}_2]$ is Hermitian, we denote that our system possesses a pseudo- \mathcal{APT} symmetry. There are no Langevin noises in our model.

For comparison, we briefly discuss the \mathcal{PT} -symmetry physics in previous studies which generally utilize the control of gain/loss, whose dynamical equation is

$$i\partial_t \begin{pmatrix} \hat{a}_1 \\ \hat{a}_2 \end{pmatrix} = \begin{pmatrix} i\delta & \kappa \\ \kappa & -i\delta \end{pmatrix} \begin{pmatrix} \hat{a}_1 \\ \hat{a}_2 \end{pmatrix} + \begin{pmatrix} \hat{f}_1 \\ \hat{f}_2 \end{pmatrix}, \quad (\text{S13})$$

where \hat{f}_1 and \hat{f}_2 are Langevin noise operators. To study the non-Hermitian physics in quantum realm, we have replaced the classic wave amplitudes by the quantum field operators. In the classical domain, these Langevin noises are removed because their zero expectation values. However, this will lead to a problem in the quantum domain where the field operator solutions without Langevin noise operators do not obey the Bosonic commutation relations. Therefore Langevin noise operators must be included in the above dynamical equation, which breaks the \mathcal{PT} symmetry.

We have focused on the dynamics of the system in the main text. To see how the quantum pseudo- \mathcal{APT} symmetry is related with the ground state of the system, we consider the second-quantized Hamiltonian $\mathcal{H} = \delta \left[\hat{a}_1^\dagger \hat{a}_1 + \hat{a}_2^\dagger \hat{a}_2 \right] + i\kappa \left[\hat{a}_1^\dagger \hat{a}_2^\dagger - \hat{a}_1 \hat{a}_2 \right]$. In the pseudo- \mathcal{APT} -broken region, the two eigenmodes read $\hat{b}_+ = \frac{\kappa}{\sqrt{2\lambda_0\delta - 2\lambda_0^2}} \langle L_+ | \vec{a} \rangle$ and $\hat{b}_-^\dagger = \frac{\kappa}{\sqrt{2\lambda_0\delta + 2\lambda_0^2}} \langle L_- | \vec{a} \rangle$. We have $\mathcal{H} = \lambda_0 (\hat{b}_+^\dagger \hat{b}_+ + \hat{b}_-^\dagger \hat{b}_-)$ and \hat{b}_\pm satisfy the bosonic commutation relation. The ground state satisfy $\hat{b}_\pm |GS\rangle = 0$, which is a two-mode squeezed state in the $\hat{a}_{1,2}$ basis, *i.e.*, $|GS\rangle = \sum_n \sqrt{1 - |q|^2} q^n |n, n\rangle$ with $q = i \frac{\delta - \lambda_0}{\kappa}$ and $|n, n\rangle$ the Fock state in $\hat{a}_{1,2}$ basis. In the pseudo- \mathcal{APT} -symmetric region, the two eigenmodes no longer satisfy bosonic commutation relation, therefore the second-quantized Hamiltonian cannot be diagonalized and has no well defined ground state. The system is always dynamically unstable and the energy of the system is not bounded from below. We want to emphasize that, here we are interested in the dynamics of the system rather than its ground state, therefore, the system is not necessarily stable or with energy bounded from below. For a physical process such as the parametric down conversion, the dynamics are well characterized by our model. In a realistic experiment, the evolution time and thereby the photon number are always finite, and the dynamical model is physical.

Recall that the squeezing factor S is defined based on the dynamical evolution of the field operators (*i.e.*, $\hat{X}_1(\varphi_+, t) \pm \hat{X}_2(\varphi_+, t) = S^{\pm 1} [\hat{X}_1(\varphi_-, 0) \pm \hat{X}_2(\varphi_-, 0)]$), therefore, S is independent of the initial state. However, the variance of $\hat{X}_1(\varphi, t) \pm \hat{X}_2(\varphi, t)$ does depend on the initial state. If we start from the state $|GS\rangle$, then the variance of $\hat{X}_1(\varphi, t) \pm \hat{X}_2(\varphi, t)$ should not change with time for all φ , since $|GS\rangle$ is the ground state of \mathcal{H} and thus $|GS(t)\rangle = |GS(t=0)\rangle$. On the other hand, the dynamics of the field operator in Heisenberg picture give $\hat{X}_1(\varphi_+, t) \pm \hat{X}_2(\varphi_+, t) = S^{\pm 1} [\hat{X}_1(\varphi_-, 0) \pm \hat{X}_2(\varphi_-, 0)]$, which indicate that the two-mode variance along φ_+ at time t is relatively squeezed with respect to the two-mode variance along φ_- at time 0. This means that the two-mode variance along φ_+ is $S^{\pm 2}$ times of the two-mode variance along φ_- for an initial state $|GS\rangle$ whose two-mode variance is time-independent. It can be shown that $|GS\rangle$, a two-mode squeezed state, does satisfy the above relation.

S3. Quantum Fisher information

We focus on the initial coherent state $|\psi_0\rangle = |\alpha_1, \alpha_2\rangle$, and the final state reads $|\psi(t)\rangle = e^{-i\mathcal{H}t} |\psi_0\rangle$ with the second-quantized Hamiltonian $\mathcal{H} = \delta \left[\hat{a}_1^\dagger \hat{a}_1 + \hat{a}_2^\dagger \hat{a}_2 \right] + i\kappa \left[\hat{a}_1^\dagger \hat{a}_2^\dagger - \hat{a}_1 \hat{a}_2 \right]$. We write $|\psi_0\rangle = \hat{D}_1(\alpha_1) \hat{D}_2(\alpha_2) |0, 0\rangle$ with displacement operators $\hat{D}_j(\alpha_j) = e^{\alpha_j \hat{a}_j^\dagger - \text{h.c.}}$ and vacuum state $|0, 0\rangle$. Now we are working in the Schrödinger picture and the time-independent field operators are $\hat{a}_j = \hat{a}_j(0)$. Then we have $|\psi(t)\rangle = \hat{D}_1(\alpha'_1) \hat{D}_2(\alpha'_2) \sum_n \sqrt{1 - |q|^2} q^n |n, n\rangle$, with $\alpha'_j = A\alpha_j + B\alpha_{\bar{j}}$, $q = \frac{B}{A^*}$ and $|n, n\rangle$ the Fock state. In particular, $|\psi(t)\rangle = [e^{-i\mathcal{H}t} \hat{D}_1(\alpha_1) \hat{D}_2(\alpha_2) e^{i\mathcal{H}t}] e^{-i\mathcal{H}t} |0, 0\rangle$. Using $e^{-i\mathcal{H}t} \hat{a}_j e^{i\mathcal{H}t} = A(-t) \hat{a}_j + B(-t) \hat{a}_{\bar{j}}^\dagger$, $A(-t) = A^*(t)$ and $B(-t) = -B(t)$, we obtain $[e^{-i\mathcal{H}t} \hat{D}_1(\alpha_1) \hat{D}_2(\alpha_2) e^{i\mathcal{H}t}] = \hat{D}_1(\alpha'_1) \hat{D}_2(\alpha'_2)$. From $\hat{a}_j |0, 0\rangle = 0$, we have $[e^{-i\mathcal{H}t} \hat{a}_j e^{i\mathcal{H}t}] e^{-i\mathcal{H}t} |0, 0\rangle = [A^* \hat{a}_j - B \hat{a}_{\bar{j}}] e^{-i\mathcal{H}t} |0, 0\rangle = 0$, thus $e^{-i\mathcal{H}t} |0, 0\rangle = \sqrt{1 - |q|^2} \sum_n q^n |n, n\rangle$, which is a two-mode squeezed vacuum state. The quantum Fisher information is calculated as $F_\kappa = 4 \langle \partial_\kappa \psi(t) | \partial_\kappa \psi(t) \rangle - 4 | \langle \partial_\kappa \psi(t) | \psi(t) \rangle |^2$ [2]. We can obtain the expression given by Eq. (7) in the main text after some algebraic manipulations.

For the sensing in the \mathcal{APT} -broken (stable) region, the final state has no squeezing (*i.e.*, $S = 1$) at the working point $t = nT$, nevertheless, the QFI possesses the divergent scaling $F_\kappa \sim (2n\pi)^2 \lambda_0^{-6}$ in the vicinity of the EP with $\lambda_0 \sim 0$ and $\lambda_0 t = n\pi$. Even we consider the squeezing during the evolution, which reaches its maximum $S_m \sim \lambda_0^{-1}$ at time $t = nT + T/2$, we have $F_\kappa \sim (2n\pi)^2 S_m^6$. Therefore, QFI can be very large without strong squeezing during the whole evolution (especially for a large n). Also, for our EP-based sensing, the sensing precision of our measurement scheme is at the same order as quantum Cramér-Rao bound set by the QFI. Our scheme works in a wide range of parameter space on the stable side of the EP. Moreover, the sensitivity as a function of evolution time reaches its peak values at the working points (*i.e.*, $t = nT$). These peaks have a large width which roughly equals to 1/4 the peak separation, thus high sensitivity can still be achieved even when the evolution time is slightly away from the working point.

In comparison, for the \mathcal{APT} -symmetric (unstable) region, we find $F_\kappa \sim e^{4\lambda_0 t} \lambda_0^{-6}$ when $e^{\lambda_0 t}$ is much larger than $e^{-\lambda_0 t}$. In the vicinity of the EP with $\lambda_0 \sim 0$, the QFI possesses the divergent scaling $F_\kappa \sim \lambda_0^{-6}$ for a fixed $\lambda_0 t$

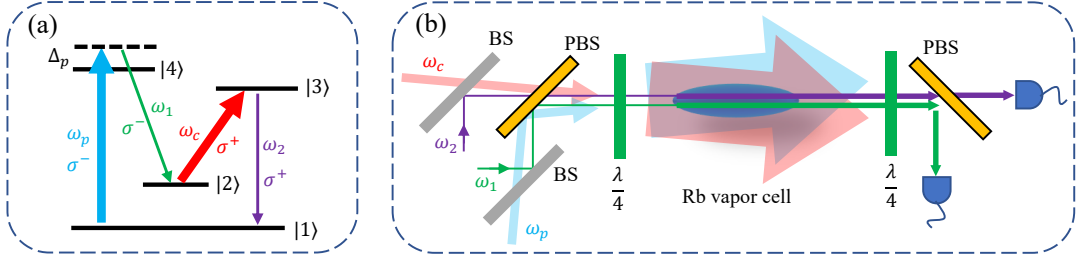


FIG. S1: Experimental realization based on nonlinear quantum optics. (a) ^{85}Rb atomic energy-level diagram: $|1\rangle = |5S_{1/2}, F = 2\rangle$, $|2\rangle = |5S_{1/2}, F = 3\rangle$, $|3\rangle = |5P_{1/2}, F = 3\rangle$, $|4\rangle = |5P_{3/2}, F = 3\rangle$. (b) Schematic of the experimental setup and geometrical arrangement of four interacting fields. BS and PBS represent the beam splitter and polarized beam splitter.

(e.g., an evolution time $\lambda_0 t = n\pi$), which is similar to the stable region. Away from the EP with $\lambda_0 \sim 1$, the QFI $F_\kappa \sim e^{4t}$ increases exponentially and can be very high after a long time. However, in the unstable region, the high QFI originates mainly from the squeezing instead of the EP, since the final state has a large squeezing factor $S \sim e^{\lambda_0 t} \lambda_0^{-1}$. In the vicinity of the EP with $\lambda_0 \sim 0$ and $\lambda_0 t = n\pi$, we have $F_\kappa \sim \lambda_0^{-2} S^4 \sim e^{-2n\pi} S^6$. Thus away from the EP with $\lambda_0 \sim 1$, we have $F_\kappa \sim S^4$. High QFI in the unstable region requires much stronger squeezing than the stable region (especially for a large n), which is generally hard to achieve in experiment since large numbers of excited particles $\sim S^2$ would be generated during the sensing process. On the unstable side of the EP, a larger λ_0 would lead to a larger QFI for a fixed evolution time, for our measurement scheme with λ_0 -dependent evolution time $t = n\pi/\lambda_0$, both the susceptibility and variance of the measured quadrature are very large, leading to a sensitivity $\Delta_\kappa^{-2} \sim \lambda_0^{-4}$ near the EP. This sensitivity is worse compared with the stable side. Therefore, for sensors working on the unstable side, new novel measurement scheme is required to reach sensitivity of the order of QFI (i.e., quantum Cramér-Rao bound). We want to emphasize that, it might be possible to operate within the unstable region for nonlinear optics, but for the BEC, it is challenging since large numbers of excitations are generated during the sensing process. Our sensing scheme, which works very well in the stable side, can be implemented in both nonlinear optics and BEC.

S4. Experimental consideration

Nonlinear quantum optics.—Our model can be realized by multi-wave mixing processes in nonlinear optical medium. Here we give more details about the experimental scheme based on four-wave mixing (the scheme based on three-wave mixing SPDC is similar). We consider the same setup as in [1], with ^{85}Rb atomic ensemble (prepared on the ground state $|1\rangle$) as the nonlinear medium. The atomic energy-level diagram, geometrical arrangement of four interacting fields and schematic of the experimental setup are shown in Fig. S1. A pump laser (ω_p) is blue detuned by Δ_p from the atomic transition $|1\rangle \rightarrow |4\rangle$ and a weak Stokes field (ω_1) follows $|4\rangle \rightarrow |2\rangle$. Another strong coupling laser (ω_c) is on resonance at $|2\rangle \rightarrow |3\rangle$ and the weak anti-Stokes field (ω_2) drives the transition $|3\rangle \rightarrow |1\rangle$. We consider resonant mixing with energy conservation $\omega_p + \omega_c = \omega_1 + \omega_2$.

The coupled equations are

$$i\partial_z \begin{pmatrix} \hat{a}_1 \\ \hat{a}_2^\dagger \end{pmatrix} = \begin{pmatrix} -\Delta k/2 & -\tilde{\kappa} \\ \tilde{\kappa} & \Delta k/2 \end{pmatrix} \begin{pmatrix} \hat{a}_1 \\ \hat{a}_2^\dagger \end{pmatrix}. \quad (\text{S14})$$

Here $\Delta k = (\mathbf{k}_1 + \mathbf{k}_2 - \mathbf{k}_p - \mathbf{k}_c) \cdot \hat{\mathbf{z}} = k_1 + k_2 - (k_c + k_p) \cos(\theta_{cp})$ is the phase mismatch with $k_j = |\mathbf{k}_j|$ the corresponding wave vector, $\hat{\mathbf{z}}$ the unit vector along propagation direction z and θ_{cp} the relative angle between the pumping and coupling beams. Δk can be tuned by slightly changing the propagation direction of the pumping or coupling beam. Typically, the wavelength of pumping (coupling) laser is 780 nm (795 nm), and $\theta_{cp} = 0.2^\circ$, so we have $\Delta k \simeq 100$ rad/m. $\tilde{\kappa}$ denotes the real nonlinear coupling coefficient [1]

$$\tilde{\kappa} = \frac{N_a \sqrt{\sigma_{13}\sigma_{24}\gamma_{13}\gamma_{14}}}{|\Omega_c|^2 + 4\gamma_{13}\gamma_{12}} \frac{\Omega_p \Omega_c}{2\Delta_p}, \quad (\text{S15})$$

where Ω_c and Ω_p are coupling and pump Rabi frequencies, γ_{ij} is the dephasing or decay rate between the states $|i\rangle$ and $|j\rangle$, N_a is the atomic density, σ_{ij} is the absorption cross section of the atomic transition $|i\rangle \rightarrow |j\rangle$. Typically, the detuning Δ_p is of the order of 100 MHz. $\tilde{\kappa}$ can be tuned by Ω_c , Ω_p and Δ_p . Δ_p is tuned by changing the frequency

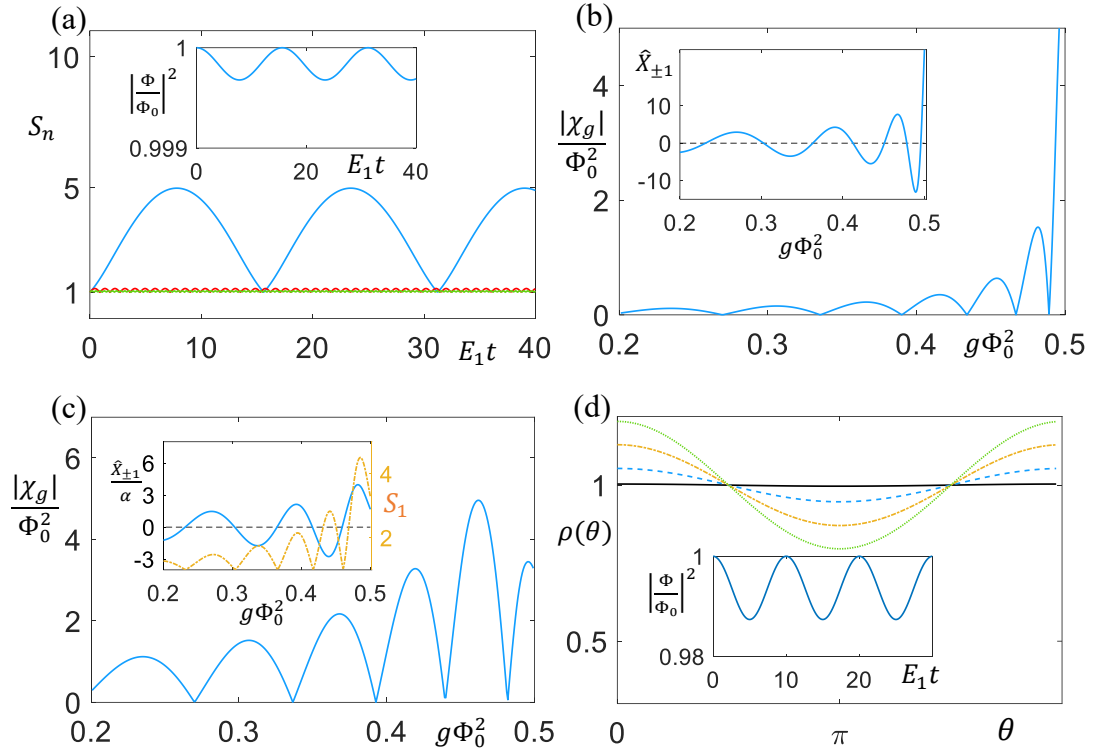


FIG. S2: Quantum sensing based on atomic BEC trapped in a ring. (a) The squeezing factors S_n as functions of evolution time for fields $\hat{\psi}_{\pm n}$ with $g\Phi_0^2 = 0.48E_1$ and $\alpha = 2$. A larger n has a weaker squeezing factor. $n = 1, 2, 3$ are shown. Inset shows how $\Phi(t)$ changes with time. (b) and (c) The susceptibility (in unit of 10^3) as a function of $g\Phi_0^2$ at time $E_1 t = 30$ for $\alpha = 2$ and $\alpha = 20$. Inset of (b) shows the corresponding quadrature. Inset of (c) shows the corresponding quadrature (solid line) and squeezing factor (dash-dotted line). (d) Density modulation along azimuthal angle θ for $E_1 t = 30$ and $\alpha = 20$. The solid, dashed, dash-dotted and dotted lines correspond to $g\Phi_0^2 = 0.46E_1, 0.462E_1, 0.465E_1, 0.468E_1$, respectively, and the corresponding quadratures and visibilities are $\langle \hat{X}_{\pm 1} \rangle = 4.41, 14.3, 29.1, 43.2$ and $v = 0.3\%, 5.3\%, 12.9\%, 20.4\%$. Inset shows the condensed atom number during the evolution for $g\Phi_0^2 = 0.46E_1$ and $\alpha = 20$.

of ω_p with the change below 100 MHz, which is enough to significantly tune $\tilde{\kappa}$. Notice that $\Delta k \propto k_p \propto \omega_p$, thus 100 MHz frequency change in ω_p only slightly modifies Δk by $\frac{100\text{MHz}}{\omega_p} \cdot \Delta k \sim 10^{-5}$ rad/m, which is negligible.

With a proper gauge choice $\hat{a}_2^\dagger \rightarrow \hat{a}_2^\dagger e^{i\pi/2}$, we obtain

$$i\partial_z \begin{pmatrix} \hat{a}_1 \\ \hat{a}_2^\dagger \end{pmatrix} = \begin{pmatrix} \delta & i\kappa \\ i\kappa & -\delta \end{pmatrix} \begin{pmatrix} \hat{a}_1 \\ \hat{a}_2^\dagger \end{pmatrix} = H \begin{pmatrix} \hat{a}_1 \\ \hat{a}_2^\dagger \end{pmatrix}, \quad (\text{S16})$$

with $\delta = -\Delta k/2$ and $\kappa = -\tilde{\kappa}$.

For the quantum sensing, we can tune Δk to the work points satisfying $\lambda_0 L = n\pi$ with $z = L$ the length of the nonlinear medium. The initial state can be obtained by injecting weak input coherent fields in \hat{a}_j (see Fig. S1), and the measurement is realized by standard homodyne detection. It can be shown that the second-quantized Hamiltonian of Eq. S14 is $\mathcal{H} = -\delta [\hat{a}_1^\dagger \hat{a}_1 + \hat{a}_2^\dagger \hat{a}_2] - \kappa [\hat{a}_1^\dagger \hat{a}_2^\dagger + \hat{a}_1 \hat{a}_2]$, which is equivalent to our previous second-quantized Hamiltonian up to a gauge transformation.

Ultra-cold atoms.—We can substitute the expansion of the BEC field operator

$$\hat{\Psi}(\theta, t) = e^{-i\mu t - i\pi/4} \Phi(t) + e^{-i\mu t} \sum_{n \neq 0} \hat{\psi}_n(t) \frac{e^{in\theta}}{\sqrt{2\pi}}, \quad (\text{S17})$$

into the nonlinear Schrödinger equation

$$i\hbar\partial_t \hat{\Psi}(\theta, t) = \left[\frac{\hat{p}^2}{2m} - g\hat{\Psi}(\theta, t)^\dagger \hat{\Psi}(\theta, t) \right] \hat{\Psi}(\theta, t), \quad (\text{S18})$$

which gives the Hartree-Fock Bogoliubov equation

$$i\partial_t\Phi = -i\frac{g}{2\pi}\sum_n\langle\hat{\psi}_n\hat{\psi}_{-n}\rangle\Phi^* - \frac{g}{2\pi}\sum_n\langle\hat{\psi}_n^\dagger\hat{\psi}_n\rangle\Phi, \quad (\text{S19})$$

$$i\partial_t\begin{pmatrix}\hat{\psi}_n \\ \hat{\psi}_{-n}^\dagger\end{pmatrix} = \begin{pmatrix}n^2E_1 - g|\Phi|^2 & ig\Phi^2 \\ ig(\Phi^*)^2 & -(n^2E_1 - g|\Phi|^2)\end{pmatrix}\begin{pmatrix}\hat{\psi}_n \\ \hat{\psi}_{-n}^\dagger\end{pmatrix} \quad (\text{S20})$$

In the stable pseudo- \mathcal{APT} -broken region, excitations are weak and $\sum_n\langle\hat{\psi}_n\hat{\psi}_{-n}\rangle$ and $\sum_n\langle\hat{\psi}_n^\dagger\hat{\psi}_n\rangle$ are much smaller than Φ^2 , therefore Φ is hardly affected by the excitations.

For the quantum sensing, we can first prepare the BEC to its ground state with $g \simeq 0$. The initial coherent state for $n = \pm 1$ can be generated by the Raman process with Laguerre-Gaussian beams carrying ± 1 orbital angular momentum. Then we increase g to the working point near the EP (*i.e.*, $2g|\Phi|^2 = E_1$). For example, we can tune g using Feshbach resonance, which in turn can be used to measure the magnetic field with ultra-high precision. The sensor operates in the pseudo- \mathcal{APT} -broken region which ensures the dynamical stability of the BEC. The squeezing and excitation number for $n > 1$ are negligible since δ increases quadratically with n . Moreover, the excitation number for $n = 1$ is generally much smaller than the number of BEC atoms, so that Φ is hardly affected during the evolution, which is confirmed by our numerical simulation. The performance of the sensor (Fig. S2) is very similar as that shown in Fig. 2 in the main text. For the measurement scheme, one can detect the density $\langle\hat{\Psi}^\dagger(\theta, t)\hat{\Psi}(\theta, t)\rangle \simeq \Phi^2 + \frac{2\Phi}{\sqrt{2\pi}}\sum_{n\neq 0}\langle\hat{X}_n(\varphi, t)\cos(n\theta) - \hat{P}_n(\varphi, t)\sin(n\theta)\rangle$ with $\varphi = -\pi/4$ and \hat{X}_n, \hat{P}_n the corresponding quadrature operators of $\hat{\psi}_n$. Notice that only $\langle\hat{X}_{\pm 1}(\varphi, t)\rangle$ and $\langle\hat{P}_{\pm 1}(\varphi, t)\rangle$ are nonzero (since the initial excitations are prepared on $n = \pm 1$) and they show divergent susceptibility with respect to g or E_1 .

In the following, we show the numerical simulations for the BEC-based quantum sensing. We find that ultra-high precision can be still achieved even if we consider weak back action of the excitations on the condensate wave function, and the long-time dynamics would still be very sensitive to system parameters around the pseudo- \mathcal{APT} transition. In Fig. S2(a), we show the squeezing factors and $|\Phi|^2$ as a function of time by solving Eq. S19 and Eq. S20 numerically. We see $|\Phi|^2$ is hardly affected even for parameters close to the exceptional point. In Fig. S2(b), we show how the quadratures $\langle\hat{X}_{\pm 1}(\varphi, t)\rangle$ and the corresponding susceptibilities change with $g|\Phi_0|^2$ (where $\Phi(0) = \Phi_0$) for $\phi = -\pi/4$. In the simulation, we set $E_1 = 1$ as the unit, and assume total atom number of the BEC is about $\Phi_0^2 = 10^5$, which is typical in experiments. We also consider an initial excited state being the coherent state with amplitudes $\alpha_{+1} = \alpha_{-1} = e^{i\pi/4}\alpha$, then we have $\hat{X}_{+1}(-\pi/4, t) = \hat{X}_{-1}(-\pi/4, t)$, and $\chi_g = \partial_g\hat{X}_{+1}$. In our simulation, we keep n up to ± 10 and check that the results are hardly affected by increasing the cutoff of n .

For our choice with $\alpha_{+1} = \alpha_{-1} = e^{i\pi/4}\alpha$, the quadratures are $\langle\hat{X}_{\pm 1}(-\pi/4, 0)\rangle = \text{Re}[e^{i\pi/4}\alpha_{\pm 1}] = 0$ and $\langle\hat{P}_{\pm 1}(-\pi/4, 0)\rangle = \text{Im}[e^{i\pi/4}\alpha_{\pm 1}] = \alpha$. The initial density reads

$$\langle\hat{\Psi}^\dagger\hat{\Psi}\rangle \simeq \Phi_0^2 + \frac{2\Phi_0}{\sqrt{2\pi}}\sum_{n=\pm 1}\langle\hat{X}_n\rangle\cos(n\theta) - \langle\hat{P}_n\rangle\sin(n\theta) = \Phi_0^2. \quad (\text{S21})$$

There is no density modulation initially. Notice that we have $\hat{P}_{+1} = \hat{P}_{-1}$ and $\hat{X}_{+1} = \hat{X}_{-1}$ for our choice of $\alpha_{\pm 1}$, $\hat{X}_{\pm 1}$ and $\hat{P}_{\pm 1}$ correspond to density and phase modulation of the wave function, and the total density is given by $\langle\hat{\Psi}^\dagger\hat{\Psi}\rangle \simeq \Phi_0^2 + \frac{4\Phi_0}{\sqrt{2\pi}}\langle\hat{X}_1\rangle\cos(\theta)$. This can also be seen from the initial total wave function which is $\langle\hat{\Psi}\rangle = e^{-i\pi/4}[\Phi_0 + i\frac{2\alpha}{\sqrt{2\pi}}\cos(\theta)]$. The initial excitation with nonzero $\hat{P}_{\pm 1}$ corresponds to phase modulation. We can define the normalized density as

$$\rho(\theta, t) = \frac{\langle\hat{\Psi}^\dagger\hat{\Psi}\rangle}{\Phi^2} \simeq 1 + \frac{4}{\Phi_0\sqrt{2\pi}}\langle\hat{X}_1\rangle\cos(\theta), \quad (\text{S22})$$

therefore, the observable $\langle\hat{X}_{\pm 1}\rangle \simeq \frac{\Phi_0\sqrt{2\pi}}{4}v$ can be detected by density imaging with $v = \frac{\max[\rho(\theta)] - \min[\rho(\theta)]}{\max[\rho(\theta)] + \min[\rho(\theta)]}$ the visibility. Around the working point, the system nearly returns to the initial state with $\langle\hat{X}_{\pm 1}\rangle \simeq 0$ and $\langle\hat{P}_{\pm 1}\rangle \simeq \alpha$, where $\langle\hat{X}_{\pm 1}\rangle$ and thereby the density modulation is very sensitive to system parameters.

For a small α (e.g., $\alpha = 2$), the excitation number and the observable $\langle\hat{X}_{\pm 1}\rangle$ are small, therefore, the density modulation is also weak, which makes the detection hard. To obtain density modulation that is easy to detect, we need to use a larger α . On the other hand, α should not be too large so that the excitation number is much smaller than the ground-state atom number and the system can still be characterized by the Hartree-Fock Bogoliubov equation. There is a trade-off in choosing α . We find that $\alpha = 20$ can lead to density modulation with visibility $\sim 20\%$, while keeping the change in condensed atom number below 2% (as shown in Figs. S2c and S2d). Such visibility could be observed using current imaging technique, and the density modulation pattern is very sensitive to parameters (e.g.,

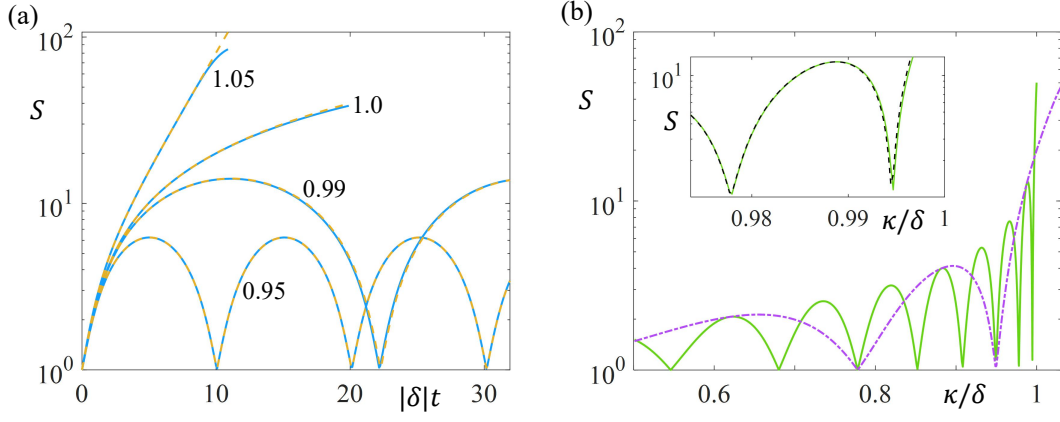


FIG. S3: Numerical simulations of the squeezing factor with Kerr interaction. (a) The squeezing factor S as a function of evolution time with $\kappa/\delta = 0.95, 0.99, 1.0, 1.05$ as labeled. The blue solid and orange dashed lines are for $U = 10^{-6}\delta$ and $U = 0$ respectively. (b) The squeezing factor as a function of κ/δ with evolution time $|\delta|t = 30$ (green solid line) and $|\delta|t = 10$ (purple dash-dotted line) with $U = 10^{-6}\delta$. The inset shows the zoom in near the EP for $|\delta|t = 30$, with black dashed line showing the $U = 0$ result. In all plots, the results for $U = 10^{-6}\delta$ are obtained in the Fock space with a cutoff photon number of 4000 in each mode, starting from the vacuum state. The results for $U = 0$ are obtained from the analytical solutions of the field operators.

the visibility changes from 0.3% to 12.9% as $g\Phi_0^2$ changes from $0.46E_1$ to $0.465E_1$). The reason why weak excitations can lead to strong modulation is that, $\rho(\theta) = 1 + v \cos(\theta)$ corresponds to a wave function $\langle \hat{\Psi} \rangle \sim \frac{1}{\sqrt{2\pi}} + \frac{v}{2\sqrt{2}} \frac{\cos(\theta)}{\sqrt{\pi}}$ (we ignore the phase modulation), and the excitation fraction [on excited state $\frac{\cos(\theta)}{\sqrt{\pi}}$] is given by $(\frac{v}{2\sqrt{2}})^2 = v^2/8$. Therefore, even for a visibility $v \sim 20\%$, the excitation fraction (or the relative change in $|\Phi(t)|^2$) is only about 0.5%. The maximum excitation fraction is reached when the quadrature $\langle \hat{X}_1 \rangle$ and also the squeezing factor S_1 reach their maximum, which is away from the working point and the corresponding susceptibility drops to 0. For $g\Phi_0^2 = 0.46E_1$ and $\alpha = 20$, the maximum excitation fraction is about 1.3% (see the inset of Fig. S2d at $E_1 t \simeq 5, 15, 25, \dots$), and the corresponding maximum visibility is about 30%.

Notice that, if we start from the exceptional point $g\Phi_0^2 = 0.5E_1$, the system will evolve back to the symmetry broken region due to the oscillation of $\Phi^2(t)$ (the oscillation is stronger for larger α), therefore, the transition at $g\Phi_0^2 = 0.5E_1$ is no longer sharp, but behaves like a crossover.

Effects of Kerr interaction.—Now we discuss the effects of Kerr interactions [3–9] $\mathcal{H}_{\text{Kerr}} = \frac{U}{2} \sum_i (\hat{a}_i^\dagger \hat{a}_i)^2$ on the dynamics near the EP. Kerr interaction strength U corresponds to the nonlinearity at the single-particle level, which is much smaller than κ . Our model can be realized by parametric down conversion and four-wave mixing in quantum optics, as well as cold atomic BECs in a ring trap. For the parametric down conversion, the typical second-order nonlinear coefficient is about 10 pm/V, and we have $\kappa = 0.5$ rad/m for typical pumping power ~ 1 W. The Kerr nonlinear index (i.e., third-order nonlinear coefficient) is typically of the order of 10^{-18} m²/W, leading to single-photon Kerr interaction strength $\sim 10^{-18}$ rad/m (i.e., $U \sim 10^{-18}\kappa$). For our proposed four-wave mixing, the ratio U/κ is given by the ratio between the power of a single photon and the pumping laser, which is about 10^{-9} (i.e., $U \sim 10^{-9}\kappa$). In the above estimation, we have assumed a beam waist of about 1 mm and the generated photons have a bandwidth of the order of MHz. For the cold atomic BEC system, we have $U \simeq \frac{\kappa}{|\Phi|^2}$. The atom number of a BEC can be up to $|\Phi|^2 \sim 10^9$ [10], which corresponds to $U \sim 10^{-9}\kappa$. For most experiments, the BEC atom number ranges from 10^5 to several 10^6 [11], corresponding to $U \sim 10^{-6}\kappa$.

In Fig. S3, we plot the numerical simulations of the squeezing factor S for $U = 10^{-6}\delta$ (δ and κ are of the same order around EP) with various evolution time t and κ/δ . Fig. S3a shows the squeezing factor as a function of evolution time with different κ/δ . We see that, the oscillation dynamics for $\kappa < \delta$ are hardly affected by the Kerr interaction. The linear and exponential increases of S for $\kappa = \delta$ and $\kappa > \delta$ remain the same when the evolution time is not too long, and the Kerr interaction would suppress the squeezing as the evolution time and squeezing factor increase. In our numerical simulation, finite number of Fock states are considered with a cutoff of 4000 photons in each mode. Numerical errors become more significant than the Kerr effects when the generated photons $\sim S^2$ is of the order of 4000, as seen at $|\delta|t > 10$ for $\kappa/\delta = 1.05$. Fig. S3b shows the squeezing factor as a function of κ/δ with evolution time $|\delta|t = 10$ and 30. We see that, the dynamics are hardly affected and squeezing factor still exhibits sharp changes at the working point of the sensor (the working point can be up to $\kappa/\delta \simeq 0.995$ for $|\delta|t = 30$). Numerical simulation

indicates that the working point of the sensor can be up to $\kappa/\delta \simeq 0.995$ even for $U \sim 10^{-6}\kappa$ as in the BEC systems. The working point can be even closer to the EP point for optical systems with much weaker Kerr interactions.

* Electronic address: Chuanwei.Zhang@utdallas.edu

† Electronic address: dusw@utdallas.edu

- [1] Y. Jiang, Y. Mei, Y. Zuo, Y. Zhai, J. Li, J. Wen, and S. Du, Anti-Parity-Time Symmetric Optical Four-Wave Mixing in Cold Atoms, *Phys. Rev. Lett.* **123**, 193604 (2019).
 - [2] L. Pezzè, A. Smerzi, M. K. Oberthaler, R. Schmied, and P. Treutlein, Quantum metrology with nonclassical states of atomic ensembles, *Rev. Mod. Phys.* **90**, 035005 (2018).
 - [3] N. Bartolo, F. Minganti, W. Casteels, and C. Ciuti, Exact steady state of a Kerr resonator with one- and two-photon driving and dissipation: Controllable Wigner-function multimodality and dissipative phase transitions, *Phys. Rev. A* **94**, 033841 (2016).
 - [4] P. Krantz, A. Bengtsson, M. Simoen, S. Gustavsson, V. Shumeiko, W. D. Oliver, C. M. Wilson, P. Delsing, and J. Bylander, Single-shot read-out of a superconducting qubit using a Josephson parametric oscillator, *Nat. Commun.* **7**, 11417 (2016).
 - [5] F. Minganti, A. Biella, N. Bartolo, and C. Ciuti, Spectral theory of Liouvillians for dissipative phase transitions, *Phys. Rev. A* **98**, 042118 (2018).
 - [6] T. L. Heugel, M. Biondi, O. Zilberberg, and R. Chitra, Quantum Transducer Using a Parametric Driven-Dissipative Phase Transition, *Phys. Rev. Lett.* **123**, 173601 (2019).
 - [7] S. Lieu, R. Belyansky, J. T. Young, R. Lundgren, V. V. Albert, and A. V. Gorshkov, Symmetry Breaking and Error Correction in Open Quantum Systems, *Phys. Rev. Lett.* **125**, 240405 (2020).
 - [8] Xin H. H. Zhang and Harold U. Baranger, Driven-dissipative phase transition in a Kerr oscillator: From semiclassical \mathcal{PT} symmetry to quantum fluctuations, *Phys. Rev. A* **103**, 033711 (2021).
 - [9] R. Di Candia, F. Minganti, K. V. Petrovnin, G. S. Paraoanu, and S. Felicetti, Critical parametric quantum sensing, [arXiv:2107.04503](https://arxiv.org/abs/2107.04503).
 - [10] D. G. Fried, T. C. Killian, L. Willmann, D. Landhuis, S. C. Moss, D. Kleppner, and T. J. Greytak, Bose-Einstein Condensation of Atomic Hydrogen, *Phys. Rev. Lett.* **81**, 3811 (1998).
 - [11] N. P. Robins, P. A. Altin, J. E. Debs, and J. D. Close, Atom lasers: Production, properties and prospects for precision inertial measurement, *Phys. Rep.* **529**, 265 (2013).
-